Report no. changed (Mar 2006): SM-225-UU

SACLANTCEN MEMORANDUM
serial no.: SM-225

SACLANT UNDERSEA RESEARCH CENTRE

MEMORANDUM


# Upper layer environmental parameters from CTD data – GIN '86 cruise

T.S. Hopkins, P. Povero
and S. Piacsek

December 1989

Page count for SM-225
(excluding covers)

| Pages | Total |
|---|---|
| i–vi | 6 |
| 1–13 | 13 |
| @1–@22 | 22 |
| | 41 |

SACLANT Undersea Research Centre
Viale San Bartolomeo 400
19026 San Bartolomeo (SP), Italy

tel: 0187 540 111
telex: 271148 SACENT I

NORTH ATLANTIC TREATY ORGANIZATION

SACLANTCEN SM-225

# Upper layer environmental parameters from CTD data – GIN '86 cruise

T.S. Hopkins, P. Povero
and S. Piacsek

---

The content of this document pertains to work performed under Project 04 of the SACLANTCEN Programme of Work. The document has been approved for release by The Director, SACLANTCEN.

Issued by:
Underwater Research Division

J.M. Hovem
Division Chief

intentionally blank page

# Upper layer environmental parameters from CTD data – GIN '86 cruise

T.S. Hopkins, P. Povero and S. Piacsek

**Executive Summary:** This memorandum presents results of analyses made on data from the first cruise of the Atlantic Inflow Experiment in June of 1986 which was designed to provide information on the entrance of Atlantic waters to the Arctic Ocean through the Faeroe–Shetland Channel. The sampling design was unique and the instrumentation was more advanced technologically than that used in previous oceanographic samplings of the area.

Detailed sampling of the oceanographic environment provides information to researchers on three levels: exploration of the environment in both space and time frames not yet observed; confirmation of our understanding of the physical laws governing the ocean environment; and utilisation of these data and laws in quantitative assessments (models) that allow environmental prediction. Such descriptions and assessments of the ocean environment are a primary goal of ASW research.

The analyses presented provide a description and synthesis of the factors affecting the propagation of sound by examining the environmental parameters that define the structure of the upper layers: the mixed layer depth, its horizontal variability, the characteristics of the propagation of sound, and certain oceanographic indicators of the distribution of energy in the upper layers of the ocean. The results are presented in both a descriptive and statistical manner. The properties of the surface mixed layer are given in a more complete manner than in any previous treatment for the southern Norwegian Sea area. Some scientific assessments are given concerning the reasons for variability in the mixed layer.

Future analyses will be conducted on the remaining data, from the 1987 Cruises, of the Atlantic Inflow Experiment. These in turn will be used in conjunction with remotely-sensed data and as input to fine-scaled oceanographic models for the evaluation of surface layer variability in the region.

intentionally blank page

SACLANTCEN SM-225

# Upper layer environmental parameters from CTD data – GIN '86 cruise

T.S. Hopkins, P. Povero and S. Piacsek

**Abstract:** The data from the SACLANTCEN June 1986 Cruise is analysed to characterise sound-propagation environment. The cruise was conducted in the Faeroese Channel and the southern Norwegian Sea as the initial cruise of the Atlantic Inflow Experiment. The sound propagation environment of the upper portion of the water column is described. The mixed layer is defined in terms of the density, Brunt–Väisälä frequency, temperature, and in terms of the sound velocity minimum. The sound-velocity profile and the characteristics of its horizontal distribution are described. The importance of wind and vertical heat flux to the mixed layer is discussed relative to its distribution.

**Keywords:** Atlantic Inflow Experiment ○ Denmark Strait ○ Faeroese Channel ○ GIN Sea ○ Greenland–Iceland–Norwegian Sea ○ horizontal variability ○ Icelandic Current ○ Iceland–Faeroe Ridge ○ mixed-layer depth ○ Norwegian Current ○ propagation ○ surface layer ○ upper layer

## Contents



**Acknowledgement:** This work was made possible by a grant from the Ocean Measurement Program of NORDA for the salary of Povero and through the concordance of the program objectives of the Applied Oceanography Group of SACLANTCEN.

# 1

# Introduction

During June 1986, the Applied Oceanographic Group (AOG) and the Ocean Engineering Department (OED) of SACLANTCEN conducted the GIN '86 Cruise in the southern Norwegian Sea, according to the AOG GIN Sea Project description[1]. The GIN '86 cruise was the first of three cruises comprising the Atlantic Inflow Experiment, the objectives of which were to describe the water mass input to the GIN Sea via the Faeroese Channel, its subsequent transitions within the Norwegian Current system, and the causes for the water mass variability throughout the region.

This memorandum contains a set of analyses consisting of an examination of the environmental parameters that define the structure of the upper layers: the mixed layer depth, its horizontal variability, the characteristics of the propagation of sound, and certain oceanographic indicators of the distribution of energy in the upper layers of the ocean.

We briefly describe the oceanographic setting and the means by which these data were taken. Next, the estimates of the surface mixed layer are given based on several different criteria, including estimates of the bulk Richardson number for the surface layer. Finally, the vertical structure of the sound velocity and its variability are described relative to the governing oceanographic parameters.

[1] SACLANTCEN Applied Oceanography Group, The GIN Sea oceanographic programme, April 1985.

# 2

# Oceanographic setting

A major reason for choosing the region and phenomenon of the Atlantic Inflow was to provide greater physical understanding on a strategically important area. The southern Norwegian Sea was known from many previous surveys to be a region of strong frontal zones and extensive meso-scale variability. The primary reason for this is that the region is the site of a large-scale convergence of Arctic and Atlantic water masses. As a consequence, convergence of much of the meso- and-small scale structure, even though generated locally, has its origin in large-scale processes. An understanding of the variability requires then a knowledge both of local energy-exchange processes and of the variability in the large-scale forcing.

In order to understand the sources of $T$-$S$ variability in the region it is profitable to characterise the local water masses and the circulations that control their distribution (for a thorough discussion, see Hopkins, 1988a). The Arctic Ocean experiences a greater atmospheric net heat loss than does the North Atlantic, causing the formation of Arctic waters having much colder temperatures than the Atlantic Waters. Consequently, the Arctic waters are more dense and are contained within the Arctic Ocean by the continental ridge that blocks deep circulation between Greenland and Scotland. As more Arctic dense water is produced every year, the accumulation pours out over the deeper part of this blocking ridge, particularly through the 800-m deep Faeroe Bank Channel. In response to this outflow, surface Atlantic water floods in, mostly in the Faeroe–Shetland Channel. The accumulation of the less dense waters on the eastern boundary (Norway) plus the mean southwesterly winds force the Norwegian Atlantic Current with a northward transport of Atlantic waters away from the region of inflow. The fact that the forces driving the inflow and those driving the Norwegian Atlantic Current are not the same causes a zone of uncoupling between them, and consequently a zone of great variability.

We define the Arctic Front as the confluence of Arctic and Atlantic waters. If there were no exchange between the two oceans, the front would create a more-or-less vertical separation and would extend parallel to the Greenland–Scotland Ridge. But there is an exchange, and where it exists the vertical separation breaks down. Because of the pressure differences caused by the differing densities of the Atlantic and Arctic water masses on either side of the front, there is a corresponding flow along the front, the Icelandic Current. This situation prevails along the middle portion of the front, along the Iceland–Faeroe Ridge, with the front being mostly vertical and the Icelandic Current flowing southeastward along it. At the western (Denmark Strait) and eastern (Faeroese Channel) ends this situation does not prevail. Through

the Faeroese Channel the Atlantic inflow overrides the front causing it to be nearly horizontal, and the Icelandic Current, confluent from the west, submerges and flows underneath the incoming Atlantic Water. The effect is that the Arctic Front lies underneath the incoming Atlantic Water, or the Norwegian Atlantic Water as it is called, after entry into the Norwegian Sea. Towards the western boundary of the Norwegian Atlantic Water, it becomes more vertical and finally intersects the surface becoming again a surface front between waters of Arctic and Atlantic origin.

North of the Faeroes the Icelandic Current becomes more complicated in the sense that it merges with an entering segment of the Atlantic Water. While the original cold branch submerges, this warm branch crosses over it and becomes part of the Norwegian Atlantic Current. Because the cold branch of the Icelandic current is transporting mostly Arctic Water of colder temperature and lower salinity than the Atlantic Water, its presence causes a pronounced thermocline and salinity minimum directly underneath the Atlantic Water. The core of this submerged Arctic Water is best identified by a salinity minimum which coincides with a sound-velocity minimum, the depth of which can vary on the order of a hundred meters as the interface between them is correspondingly distorted by the local dynamics.

The simple picture that we have described involves a zone of convergence of three principal water masses in the southeastern Norwegian Sea: a deep Arctic water outflowing through the Faeroe–Shetland Channel, an Atlantic surface water flooding in on the Norwegian side, and an Arctic surface water that flows southeastwards along the Iceland–Faeroe Front. The latter two are surface waters and are the primary components of the surface mixed layer in the frontal regions where the two water masses coexist. A fourth component of lower salinity is contained over the Norwegian Shelf by the Norwegian Shelf Front and is composed of a mixture of Norwegian coastal run-off, Baltic Sea effluent, and Norwegian Atlantic Water.

# 3

## The data

The water-property sampling during GIN '86 was was made by means of a Neil Brown Instruments Systems Mk III CTD which recorded data at 32 Hz from attached temperature, conductivity, pressure, dissolved oxygen, and transmittance sensors. This package was lowered at 1 m/s to obtain vertical profiles of these parameters and then was raised to discrete depths at which water samples were taken for laboratory analyses. These data were first edited, ordered in pressure, and calibrated before calculating the various dependent variables and averaged to 1-m intervals. Data acquisition is normally begun with the CTD sensors 1–3 m below the sea surface; a polynomial extrapolation routine was used to extend the data to the zero depth. A description of the cruise and the data processing, included in the cruise report (Hopkins, 1988b).

A total of 144 stations were taken during the second leg of GIN '86 as shown in Fig. 1, although some were taken as repetitions or time series. To illustrate the oceanographic setting in the context of this sampling, we present a few of the data results (further detail is given in Hopkins 1988b). The surface flow as determined by the density field is shown in Fig. 2. The main branch of the Atlantic Inflow proceeds through the Faeroe–Shetland Channel and along the Norwegian Slope. Its presence is manifested by warmer and more saline waters (8–10 °C, > 35.2 ppt) and normally the core of the inflow is concentrated over the Shetland Slope as shown in Figs. 3a, 3b and 3c. Such a distribution causes strong horizontal gradients in the sound velocity, e.g. up to 1 m/s/km at 400 m depth. The deep sound channel is much better developed on the Faeroes side of the channel (Fig. 3d).

The other main input to the region comes from the Atlantic Water portion of the Icelandic Current which turns northeastward to form a westward branch of the Norwegian Atlantic Current. A northward cross-section across the Faeroes Slope (Figs. 4a and 4b) demonstrates some of the complication caused by entrance of the Icelandic Current, which from Figs. 2 and 4c, can be seen to be more complicated than the Faeroe–Shetland inflow (Fig. 3). In the upper layer the salinity distribution has two maxima which indicates some spatial division in the Atlantic Water entering north of the Faeroes. In fact, the velocity section (Fig. 4c) shows the two cores to be separated by a return flow (to northwest). This division can be seen to effect a downbowing of the isotherms and to substantially weaken the sound-velocity minimum (i.e. in Fig. 4d between Stations 112 and 113).

# 4

# Mixed-layer depth

From the point of view of internal wave motion, the 'mixed layer' is an upper boundary region through which internal waves cannot propagate for lack of a gravitational restoring force, i.e. a vertical layer without stratification. From the point of view of sound propagation, the 'mixed layer' is a surface layer in which the sound velocity increases to a sub-surface maximum. This can occur when either the gradients of temperature and salinity are sufficiently small such that the pressure dependence causes the sound velocity to increase; or it can occur in the rather unusual case when the temperature and salinity have positive gradients. The lack of vertical gradients within a surface layer is normally attributed either to mechanical mixing, due to the turbulence breaking of surface waves and/or to shear turbulence at the top of the pycnocline, or to convective mixing due to the production of dense surface waters as a result of buoyancy loss to the atmosphere. For surface waves, the depth of mixing is roughly limited to half of the surface wavelength; and for convection, the depth is limited by the intensity of the atmospheric losses and by the strength of the sub-surface pycnocline.

Thus the mixed-layer depth (MLD) can be defined in several ways. If the propagation of internal waves is of interest, some criteria on the stratification might be used; or if acoustic sound propagation is of interest, the depth of the sound-velocity maximum would be the most straightforward means. However, because the temperature is numerically dominant in the sound-velocity dependency and because the temperature is more easily and more often measured, i.e. with XBTs, a criterion on the surface temperature gradient is most often used to determine the mixed-layer depth. On the other hand, from the point of view of the gravitational stability of the surface waters, a criterion on the density gradient is more accurate. Below, we compare some of the different methods (following the approach of Molinelli, Donelson, and Lilly, 1981) to provide a more complete description of this surface phenomena. The statistics for the various parameters referenced are given in Table 1.

$\mathrm{MLD_d}$ *from* $\sigma_t$ The $\mathrm{MLD_d}$ was taken as the depth at which the density $\sigma_t$ exceeded the surface value by 0.02 units. The distribution (Fig. 5) shows strong variability, particularly in the inflow area. The Fig. 5 insert shows bimodal split in the percentage distribution (also Table 1) of 9 and 29 m, an average of 24 m, and is skewed towards a maximum at 76 m.

$\mathrm{MLD}_N$ *from Brunt–Väisälä frequency* The $\mathrm{MLD}_N$ was defined as the uppermost depth at which the Brunt–Väisälä frequency $N$ exceeded 2 cycles/h. A similar

**Table 1** *The statistics for the observed and calculated mixed-layer depth parameters given in the text*

| Parameter | Mode | Mean | St. Dev. | Max. | Min. |
|---|---|---|---|---|---|
| *A. All stations* | | | | | |
| $MLD_d$ | 9,29 | 23.5 | 16.5 | 76 | 1 |
| $MLD_N$ | 3 | 20.0 | 14.1 | 68 | 1 |
| $MLD_t$ | 31 | 27.2 | 18.2 | 84 | 3 |
| $MLD_c$ | 2 | 18.0 | 16.7 | 65 | 0 |
| $SV_{max}$ | – | 1488.1 | 3.1 | 1498 | 1478 |
| $SV_{min}$ | 1469.7 | 12.9 | 1490 | 1454 | |
| depth $SV_{min}$ | – | 430.2 | 249.1 | 910 | 25 |
| $SV_{max} - SV_{min}$ | – | 18.3 | 12.8 | 39 | 0 |
| Ri number | – | 8.2 | 9.6 | 73 | 0.1 |
| *B. Region 1* | | | | | |
| $MLD_d$ | 9,29 | 22.4 | 13.5 | 64 | 3 |
| $MLD_N$ | 9 | 18.6 | 10.4 | 51 | 3 |
| $MLD_t$ | 31 | 24.9 | 14.2 | 67 | 3 |
| $MLD_c$ | 2 | 15.1 | 13.4 | 60 | 0 |
| $SV_{max}$ | – | 1487.8 | 3.2 | 1498 | 1478 |
| $SV_{min}$ | – | 1458.2 | 1.6 | 1463 | 1454 |
| depth $SV_{min}$ | – | 624.3 | 106.4 | 910 | 390 |
| $SV_{max} - SV_{min}$ | – | 29.6 | 3.4 | 39 | 19 |
| Ri number | – | 9.4 | 11.0 | 73 | 1 |
| *C. Region 2* | | | | | |
| $MLD_d$ | 4 | 24.8 | 19.5 | 76 | 1 |
| $MLD_N$ | 3,4 | 21.7 | 17.3 | 68 | 1 |
| $MLD_t$ | 11 | 29.8 | 21.5 | 84 | 3 |
| $MLD_c$ | 0 | 21.5 | 19.4 | 65 | 0 |
| $SV_{max}$ | – | 1488.4 | 19.4 | 1496 | 1482 |
| $SV_{min}$ | – | 1483.4 | 4.0 | 1490 | 1473 |
| depth $SV_{min}$ | – | 200.4 | 156.9 | 645 | 25 |
| $SV_{max} - SV_{min}$ | – | 5.0 | 3.8 | 18 | 0 |
| Ri number | – | 6.7 | 7.3 | 37 | 0.1 |

distribution is shown in Fig. 6 with a slight shift towards shallower values, with an average of 20 m (Table 1).

$MLD_t$ *from temperature* According to convention in defining the mixed layer with XBT data, the $MLD_t$ was taken as the first depth at which the temperature incremented by 0.2 K (Warn-Varnas, Dawson, Martin, 1981). Although the areal distribution (Fig. 7) demonstrates the same features, it can be seen from the histogram that the $MLD_t$ is generally deeper with an average of 27 m.

$MLD_c$ *from* $SV_{max}$ In this case the $MLD_c$ was defined as the depth of the uppermost maximum in the sound-velocity profile. The areal distribution is shown in Fig. 8.

The frequency histogram (Fig. 8 insert) shows a bimodal distribution with a paucity of stations having MLDs of $\sim$ 15 m, with an average of 18 m, and skewed towards the deeper values up to 65 m.

*Correlations* Figure 9 provides the correlations between the $\mathsf{MLD}_N$, $\mathsf{MLD}_c$ and $\mathsf{MLD}_t$ and the $\mathsf{MLD}_d$. Effectively the criteria for $\mathsf{MLD}_N$ is more stringent than that for $\mathsf{MLD}_d$, hence occasionally $\mathsf{MLD}_d$ will exceed that of $\mathsf{MLD}_N$, as in Fig. 9a. On the other hand, the temperature criteria is less stringent, causing the $\mathsf{MLD}_t$ to be sometimes deeper than the $\mathsf{MLD}_d$ (Fig. 9b). The scatter in that of $\mathsf{MLD}_d$ *vs* $\mathsf{MLD}_c$ (Fig. 9c) is due to the fact that the SV is numerically more noisy such that first maxima do not always correspond to the depth of the mixed layer as defined by the density variable.

*Low-frequency cut-off* The trapping of acoustic energy in the mixed layer is frequency dependent in the sense that for any MLD there is a frequency below which the wavelength is too long to be refracted upward and trapped. This is called the low-frequency cut-off (cf. Urick, 1983; Porter, Piacsek, Henderson and Jensen, 1989) and is given by

$$f = 1500/(0.008 \times H^{3/2}).$$

Figure 10 shows the distribution of this cut-off frequency contoured at only three levels. Surface trapping for frequencies $< 5000$ Hz was possible only over the center portions of the sampled domain, being blocked by the higher cut-off frequencies (shallower MLD) of the frontal and/or shelf regions.

*Bulk Richardson number* Ri The Richardson number is often used as a criterion to determine if the eddy kinetic energy for a mass (or volume) is likely to increase or not. This is done by comparing the gravitational stability of a layer, which acts to inhibit turbulence, with the mean velocity shear through the layer, which tends to generate turbulence. This can be expressed in a non-dimensional form:

$$\mathsf{Ri} = \frac{g}{\rho}\frac{\partial \sigma_t}{\partial z}\left(\frac{\partial u}{\partial z}\right)^{-2}.$$

We have approximated this for the mixed layer by assuming that the MLD $= \Delta z$ and that the velocity shear was only that due to the wind such that it decreased from 1% of the wind speed at the surface to zero at the bottom of the MLD. The spatial and frequency distributions of Ri are shown in Fig. 11. The distribution is not recognisably similar to that of, say, the $\mathsf{MLD}_d$ (Fig. 5) because of the additionally uncorrelated dependence on the wind speed. However, with a few exceptions, most of the area had values of $< 10$. This information is repeated in the histogram of Ri which had a strong mode at the value of 9 and was skewed toward higher values that were associated with the regions where either the wind was low or the MLD deep. In contrast, the area of the Norwegian Shelf (Stations 90–96 in Fig. 1) had $\mathsf{Ri} < 1$ due to high winds and low MLDs. Generally any Ri numerically greater than one is indicative of insufficient kinetic energy to support turbulence. We note that the

value of bulk Richardson number thus calculated is usually larger and less variable than that of a locally calculated value, e.g. where over a much smaller vertical scale ($< 1$ m) the shear may be large or the stability small.

*Wind* The mean wind speeds, as determined from the corrected ship's winds (Fig. 12a), were fairly evenly distributed about the mean of 8.7 m/s (17 kn). However, these winds were not evenly distributed in time, but blew strongly at intermittent intervals throughout the cruise, as shown in Fig. 12b. With strong winds occurring so frequently, one might expect to find MLDs more evenly distributed than those determined by the above observational criteria; i.e. that the winds would maintain a fairly deep mixed layer.

*MLD calculated* To illustrate further the effect of wind on the MLD, we have calculated the MLD using the Mellor–Yamada wind-dominated mixed-layer approximation of

$$\mathrm{MLD_{MY}} = C[\tau/\rho f N]^{1/2},$$

where $f$ is the Coriolis parameter, $\tau$ the wind stress, and $C$ is a non-dimensional constant equal to 0.019 for a critical Ri = 0.23 (Martin, 1976). In this case the Brunt–Väisälä frequency $N$ was determined from the 10-m density gradient immediately below the $\mathrm{MLD_d}$. The results for all stations are shown in Fig. 13a. A better agreement is obtained for the winds greater than the mean (Fig. 13b), even though the $\mathrm{MLD_{MY}}$ values are considerably deeper. A smaller value of $C$ (e.g. $C \sim 0.01$) eliminates the $\sim$ 25-m offset in Fig. 13b. For the winds lesser than the mean (Fig. 13c), the agreement is worse. The most obvious implication of this discrepancy is that the formula is more valid for stronger winds and that the value of $C$ should be empirically chosen to match the characteristic Ri field.

*Vertical buoyancy flux* To understand the discrepancies noted in the above two paragraphs, one must consider the vertical flux of buoyancy into the mixed layer from below, i.e. through vertical motions not taken into account in conventional formulations of mixed-layer models. A detailed explanation is beyond the scope of this memorandum, but we offer as supporting evidence the following points:

1. With the much larger atmospheric scales (for spatial variations in the wind speed) it is unlikely that the wind momentum alone could be responsible for 2- to 5-fold increases in the MLD over horizontal distances of 10 km. Nor is it likely that these variations are due to the temporal variations in the wind speed. That is, with a surface wind stress fluctuating at the same or shorter timescale (hours) than the time required to generate the MLD, it is unlikely that the MLD comes in equilibrium with the wind forcing, in which case the MLD reflects some weighted time history of the wind stress. Hence, the MLD variability is not well explained by surface forcing alone.
2. The shallower MLDs were correlated with the greater sub-MLD stabilities, as shown in Fig. 14, where the MLDs are plotted against the density gradient in the 10 m immediately below the MLD. Nearly all the stations fell within the

standard error of the linear regression. The exceptions were those cases which had both a very strong density gradient and a very shallow MLD, these cases appear to have different dependency.

3. If vertical motions play a significant role then one would expect some correlation between the MLD and the depth of the $SV_{min}$. For the fundamental internal mode they would be in phase and for higher modes they would be out of phase or uncorrelated. That is, for a quasi-geostrophic feature, which is in relative steady state compared to the ship's sampling, the fundamental mode of vertical motion would raise (or lower) both interfaces simultaneously and for the second mode the displacement of the interfaces would be out of phase. In Fig. 15 the depths of the two interfaces are compared for Region 1 (where the deep $SV_{min}$ existed). For some sequences of stations they are will correlated, either negatively or positively. Examples are given in the two inserts, which provide expanded views of sampling zones in which the two depths were well correlated either out of phase (Fig. 15a) or in phase (Fig. 15b) corresponding to the first and the fundamental internal modes, respectively. Also, included in the inserts are the wind speeds for comparison.

# 5

## Sound-speed characteristics

*Surface* $SV_{max}$ The surface $SV_{max}$ was fairly evenly distributed (Fig. 16) with the mean and mode being nearly equal at a value of 1487 m/s (Table 1(B)).

$SV_{min}$ Below the $SV_{max}$ the sound velocity decreases to a minimum. The first and major part of this decrease is due to the effect of a decreasing temperature, and the second part is due to a decrease in salinity to a minimum due to the presence of the Arctic water. This generalisation holds for the deeper portions of the sampled domain, that is excluding the water columns that are entirely Atlantic water to the south and along the Shetland continental shelf where the $SV_{min}$ was not well defined or was at the bottom depth (Fig. 17).

As a consequence the total distribution of the depth of the $SV_{min}$ was distinctly bimodal (Fig. 17), where the normal distribution about 1458 m/s belongs to the cold Arctic Intermediate Water and the skewed distribution about the mode at 1487 m/s belongs to the warmer Atlantic Water. We define these as Regions 1 and 2, respectively; Table 1b gives the statistics separately for each.

The bimodal structure is not reflected in the frequency distribution of the $SV_{min}$ (insert to Fig. 16). This is because the large variability of the depth of the salinity minimum in Region 2, together with the depth variability associated with the $SV_{min}$ in Region 1, caused the combined distribution to be fairly evenly skewed towards shallower depths with the exception of a peak at 150 m that corresponded to the bottom depth of the stations taken over the continental shelf.

Finally, if we consider the difference between the $SV_{max}$ and the $SV_{min}$, as an indication of the the strength of the downward refraction occurring in the deep sound channel, we find the strongest gradient where the Icelandic Current enters the domain (Fig. 19). The bimodal distribution (insert to Fig. 19) is not surprising given the two distributions involved (Figs. 16 and 18), but it does suggest that the mechanisms determining the $SV_{max}$ are independent of those determining the $SV_{min}$.

# 6

# Conclusions

We have attempted to illustrate the range of variability in some of the environmental acoustic parameters observed during June 1986 in the southern Norwegian Sea. The variability is created by the confluence of Atlantic and Arctic water masses, by complicated bathymetry, and by strong meteorological forcing.

The results of various criteria for determining the MLD were compared. The difference between them was slight, such that any one might be used with confidence. However, if both temperature and salinity are available, the density criterion would be preferable over that of the Brunt–Väisälä frequency or that of the sound-velocity maximum, both of which tend to be more susceptible to noisy data. If only temperature is available, the temperature criterion would return results nearly as reliable as that of the density.

The $\mathrm{MLD}_d$ had a mean for the sampled region of 24 m but varied from a minimum of 1 m to 76 m. The areas of shallow MLD corresponded to the frontal zones of the Iceland–Faeroes Front or the Norwegian Shelf Front or were zones of upwelling; whereas the deeper MLD corresponded to zones of downwelling. As a result of the distribution of the MLD, a surface sound channel ($< 5$ kHz) existed proceeding from the Faeroe–Shetland Channel northeastward along the 1000–2000 m isobaths of the Norwegian Slope.

The winds during the cruise averaged 8.7 m/s and varied to peaks of and never fell below 2 m/s during the sampling interval. Despite this wind energy, the MLDs were shallower and more variable than one would expect from a simple wind-dominated mixed-layer formulation for the MLD. Some of this may have been to local heating which was at its seasonal maximum during the cruise but the effect was not measured nor observed in the near-surface temperature profiles due to the strong surface-wave mixing. The bulk Ri number for the MLD was typically around the value of 10. The sound-speed profiles had deep minima except in the areas of the homogeneous Atlantic Water or in shallow depths. In the Norwegian Sea this minimum varied in depth by 100 m about a mean of 625 m.

The vertical motions appeared to play a role roughly equivalent to the wind stress in determining the MLD. MLDs calculated as a function of the wind stress and (inversely) the stability returned only fair agreement, which did, however, improve with wind strength. Nearly the same degree of agreement was obtained with a simple correlation between the MLD and the sub-MLD density gradient. The implication

deduced was that the cases of strong density gradients were evidence of upwelling motions, i.e. that the gradients were being sustained by an upward advection against their destruction through the action of wind mixing. On the contrary, excessively deep MLDs were considered to be the result of downwelling motions. Because such vertical motions can have large amplitudes at diverse periodicities observational confirmation is difficult. It was demonstrated that on occasion there was a very strong positive correlation between the MLD and the depth of the sound-velocity minimum as would be expected if most of the vertical kinetic energy were in the fundamental mode and at other times a strong negative correlation as one might expect for higher modes. The primary difficulty in verifying this concept with the given data set was that the observations could substantiate only low-frequency distortions of the vertical structure. It is considered that the cause of these distortions is the result of Ekman pumping by the local wind-stress curl and/or the vertical motions associated with meso-scale quasi-geostrophic features in the circulation of the Norwegian Atlantic Current.

# References

Hopkins, T.S. The GIN Sea, Review of physical oceanography and literature from 1972, SACLANTCEN SR-124. La Spezia, Italy, SACLANT Undersea Research Centre, 1988a.

Hopkins, T.S. Atlantic inflow experiment: GIN Sea Cruise 86: Part I, Hydrography, SACLANTCEN SM-209. La Spezia, Italy, SACLANT Undersea Research Centre, 1988b.

Martin, P.J. A comparison of three diffusion models of the upper mixed layer of the ocean, NRL Memorandum Report 3399. Washington, D.C., Naval Research Laboratory, 1976.

Molinelli, E.J., Donelson, J. and Lilly, L. Mixed layer depth distributions from SVSTD data, TR-271. NSTL Station, MS, U.S. Naval Oceanographic Office, 1981.

Porter, M., Piacsek, S., Henderson, L. and Jensen, F.B. Acoustic impact of upper ocean models, SACLANTCEN SM-227. La Spezia, Italy, SACLANT Undersea Research Centre, 1989.

Urick, R.J. Principles of Underwater Sound. New York, NY, 3rd edition, McGraw-Hill, 1983.

Warn-Varnas, A.C., Dawson, G.M. and Martin, P.J. Forecast and studies of the oceanic mixed layer during the MILE Experiment. *Geophysical and Astrophysical Fluid Dynamics*, **17**, 1981: 63–85.

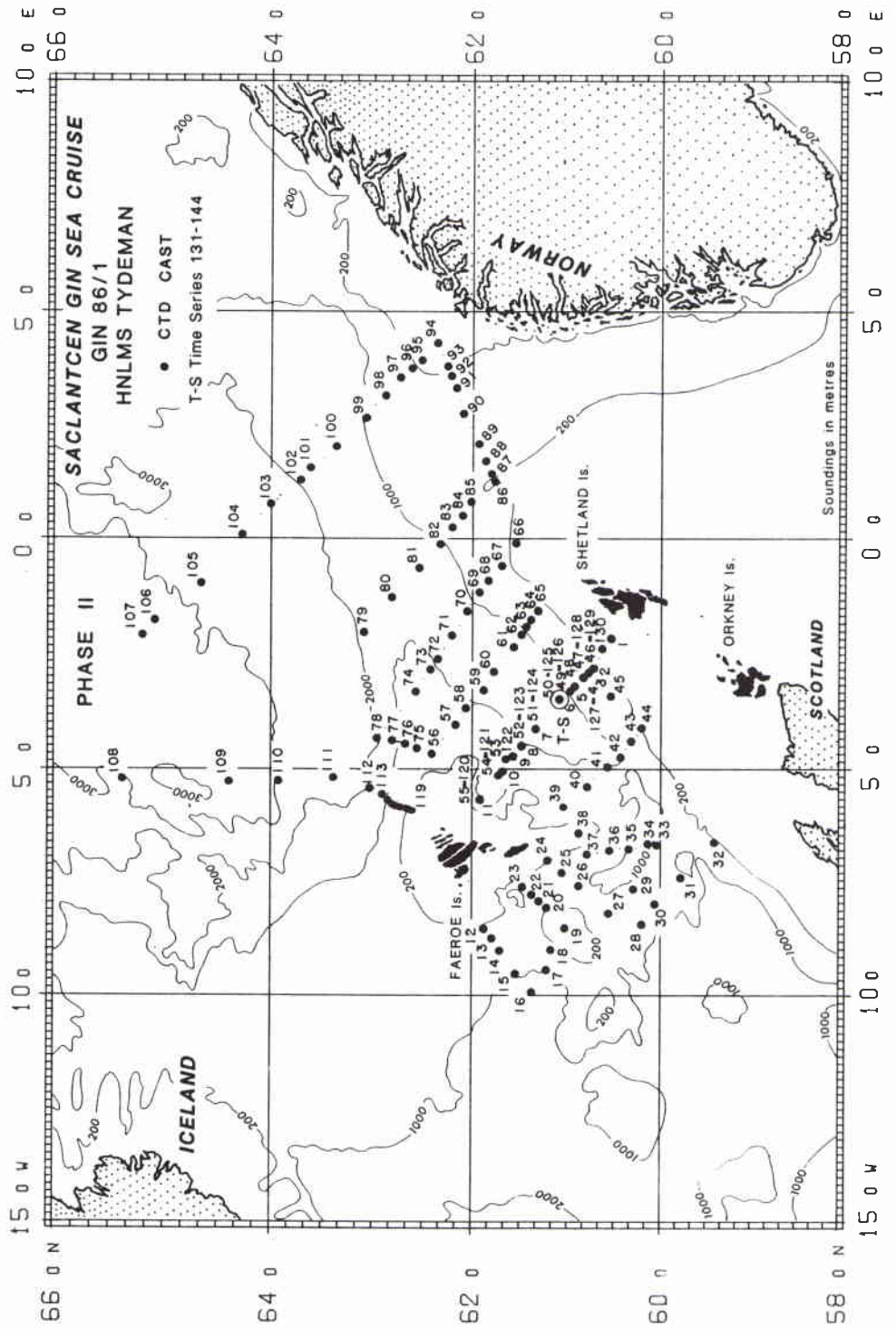


**Figure 1** *Location of CTD stations from the Leg II of the GIN '86 Cruise.*

intentionally blank page

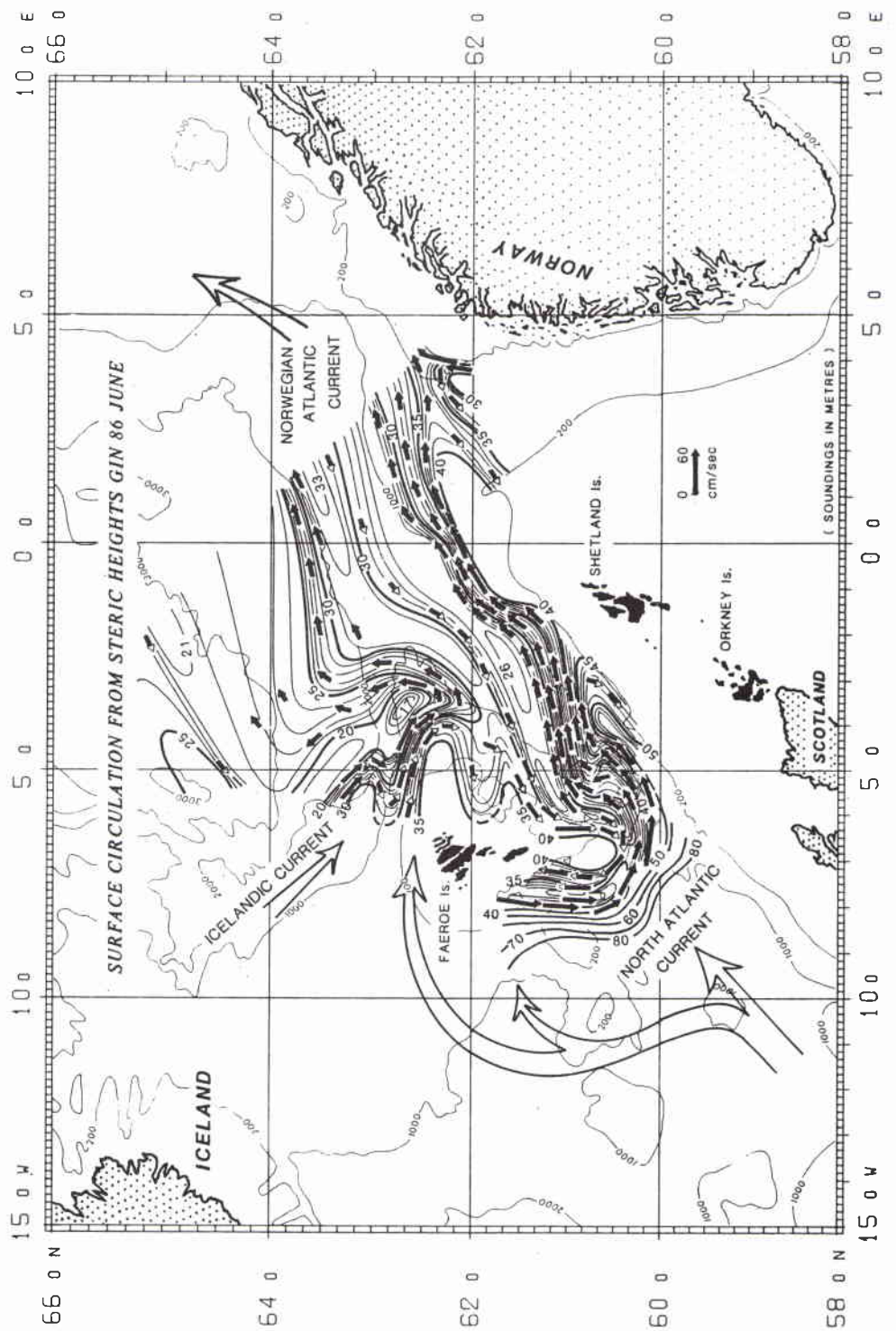


**Figure 2** *The surface circulation as calculated from the observed density field. The major currents are indicated by broad, open arrows.*

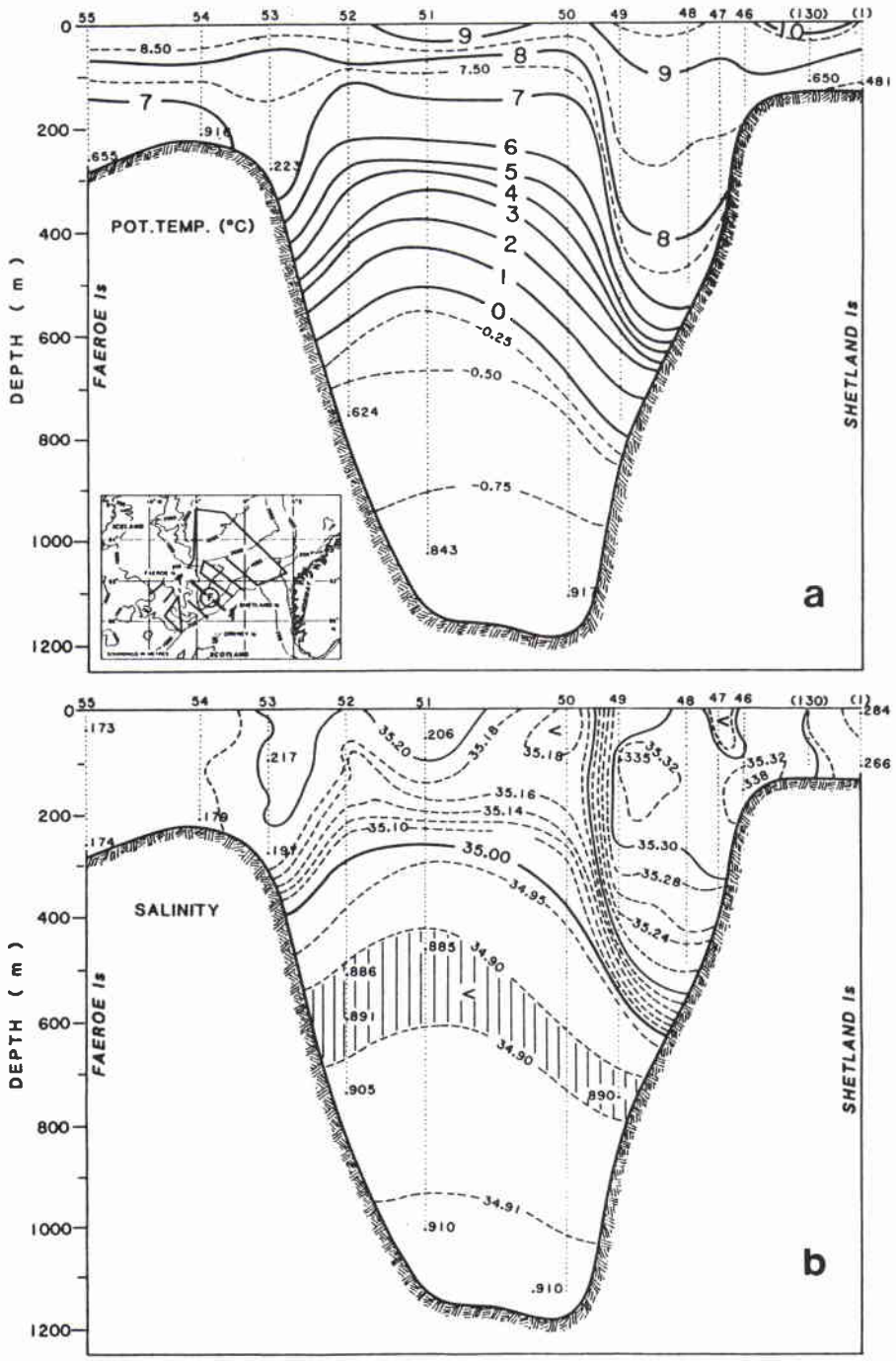


**Figure 3** *The Faeroe-Shetland transect (Stations 46–55 of Fig. 1): (a) temperature, (b) salinity, (c) velocity, (d) sound velocity.*

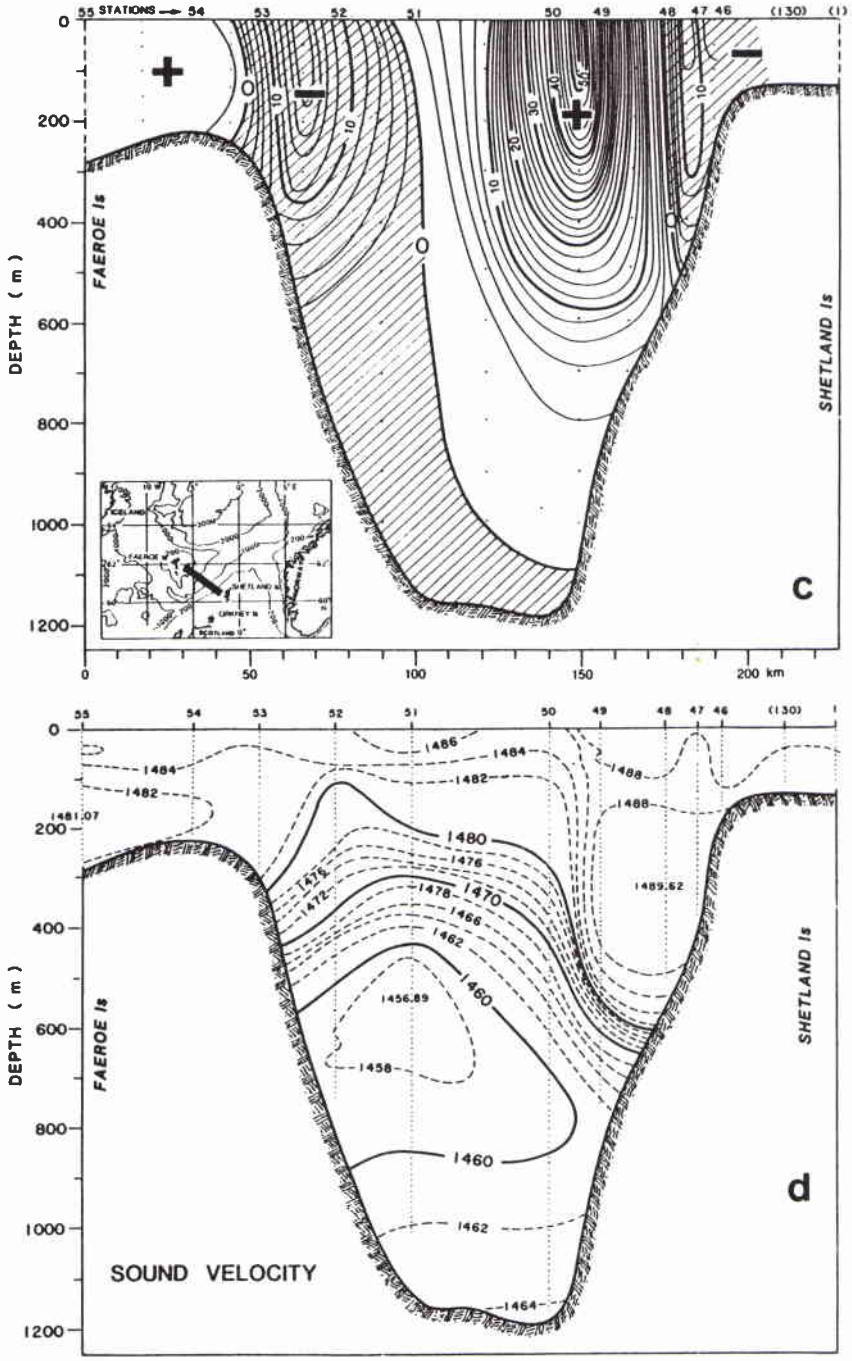
55 STATIONS → 54
53
52
51
50
49
48
47
46
(130)
(1)
DEPTH ( m )
FAEROE Is
SHETLAND Is
c
0
50
100
150
200 km
1484
1482
1480
1476
1470
1466
1462
1460
1458
1456.89
1488
1489.62
1481.07
d
SOUND VELOCITY

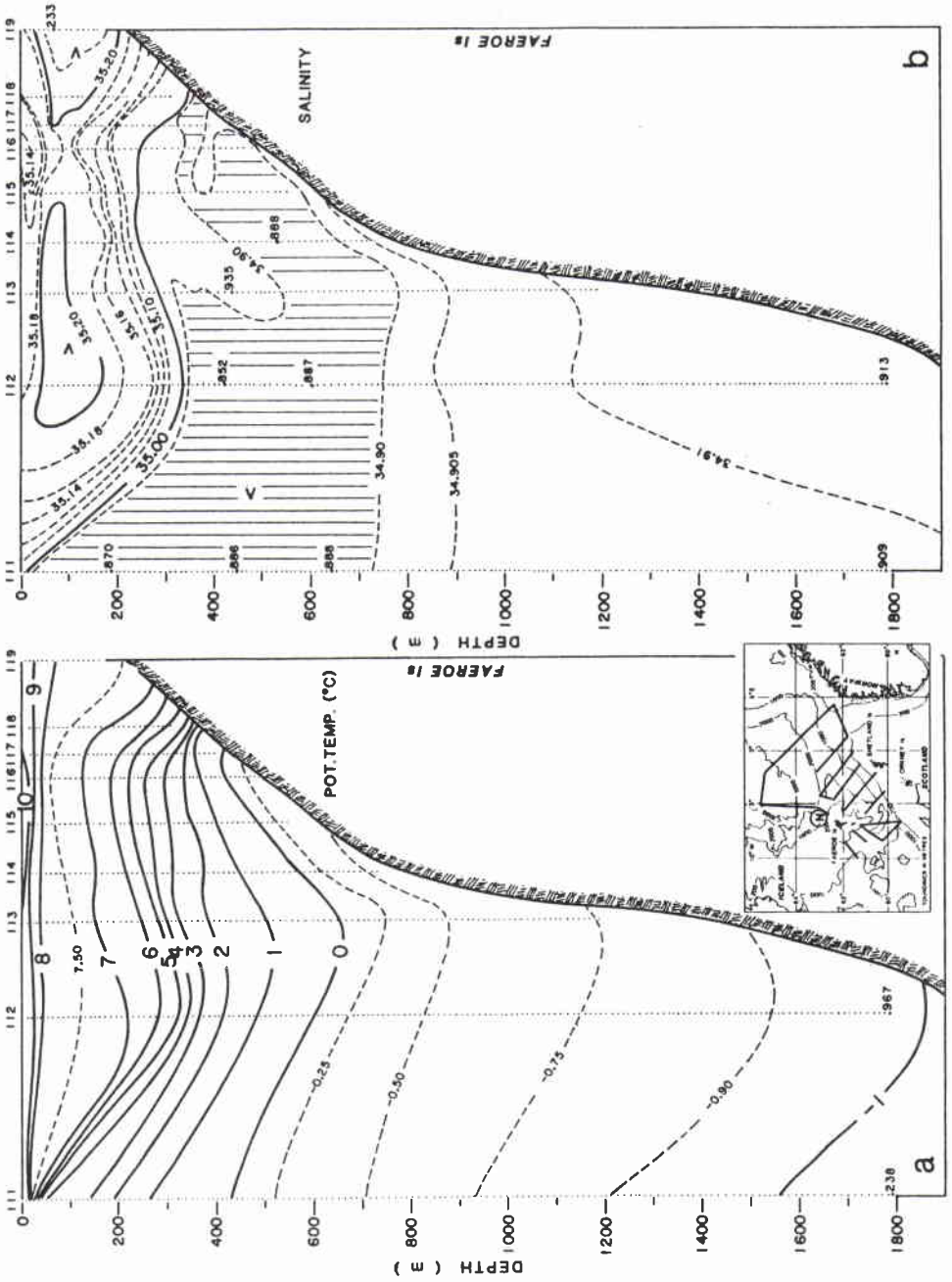


**Figure 4** *The Faeroe Slope transect (Stations 111–119 of Fig. 1): (a) temperature, (b) salinity, (c) velocity, (d) sound velocity.*

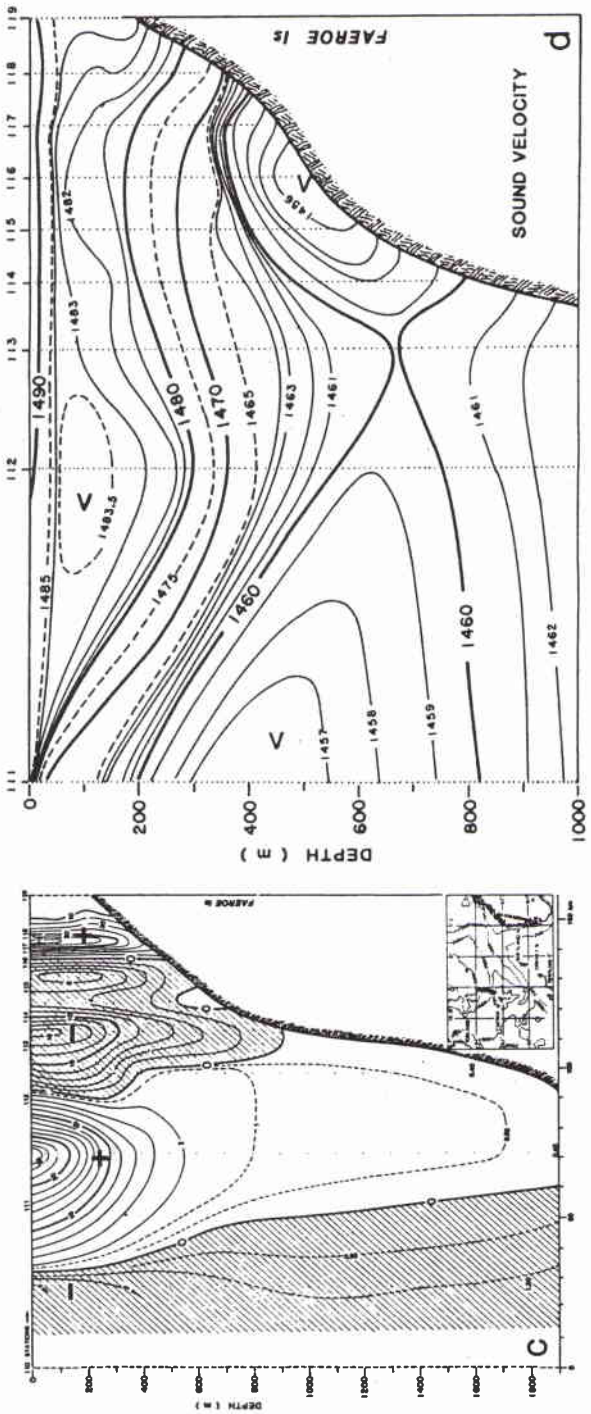
d
SOUND VELOCITY
FAEROE Is
DEPTH ( m )
0
200
400
600
800
1000
1490
1485
1480
1475
1470
1465
1463
1461
1460
1459
1458
1457
1462
1483.5
1482
1483
1456
V
C

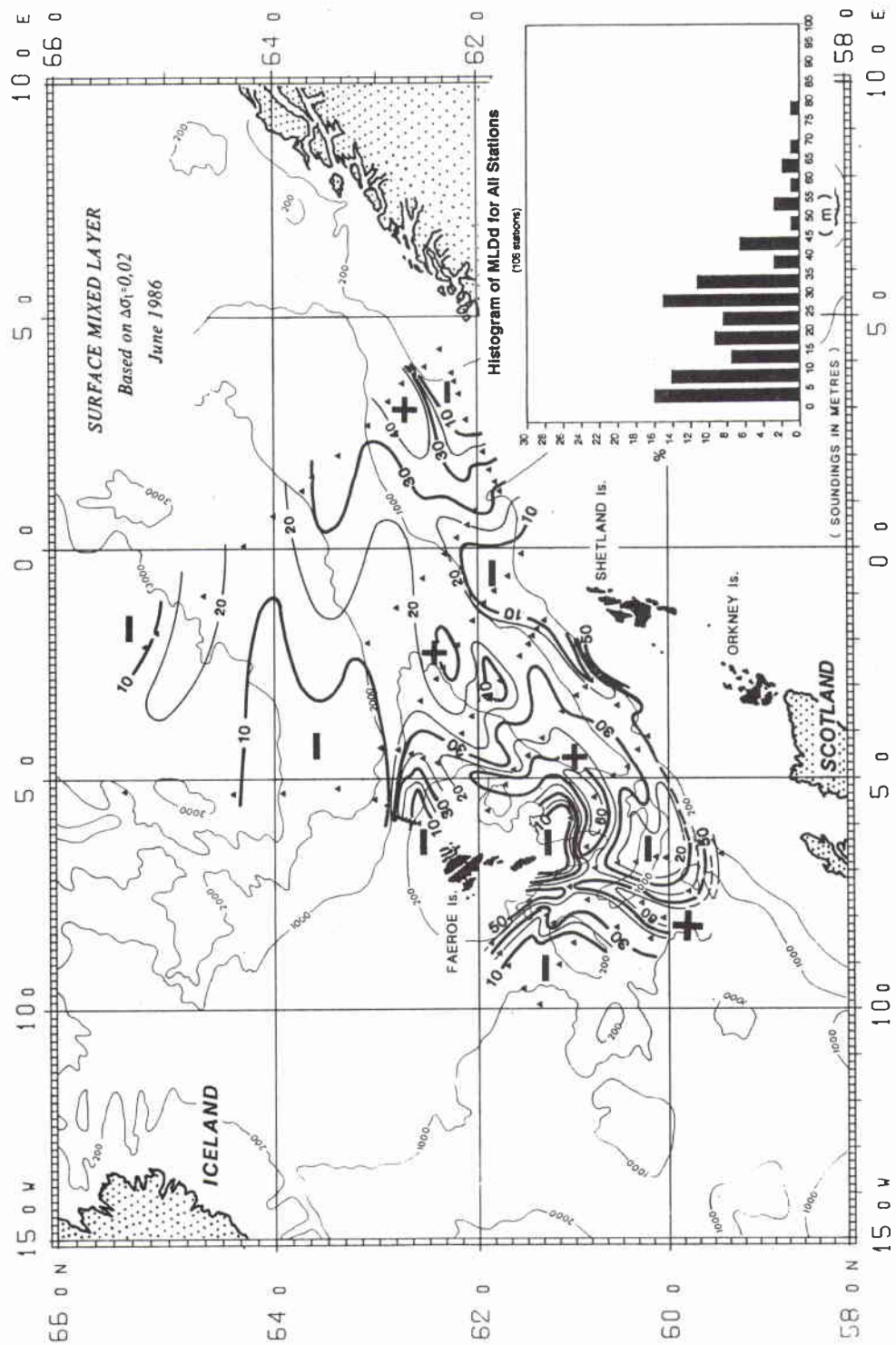


**Figure 5** *The distribution of the* MLD *as determined by the density, with the insert displaying the percentage distribution.*

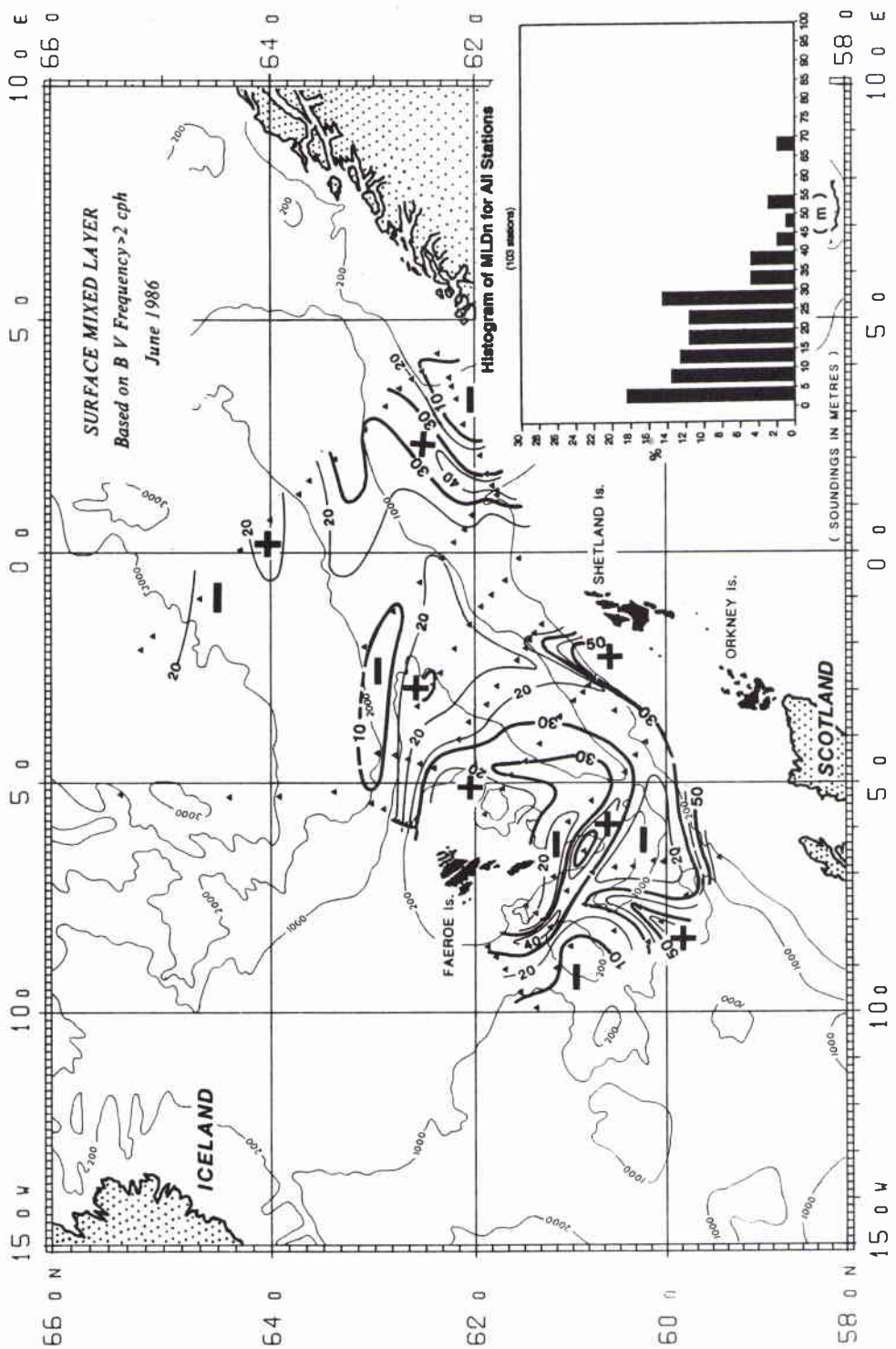


**Figure 6** *The distribution of the* MLD *as determined by the Brunt–Väisälä frequency, with the insert displaying the percentage distribution.*

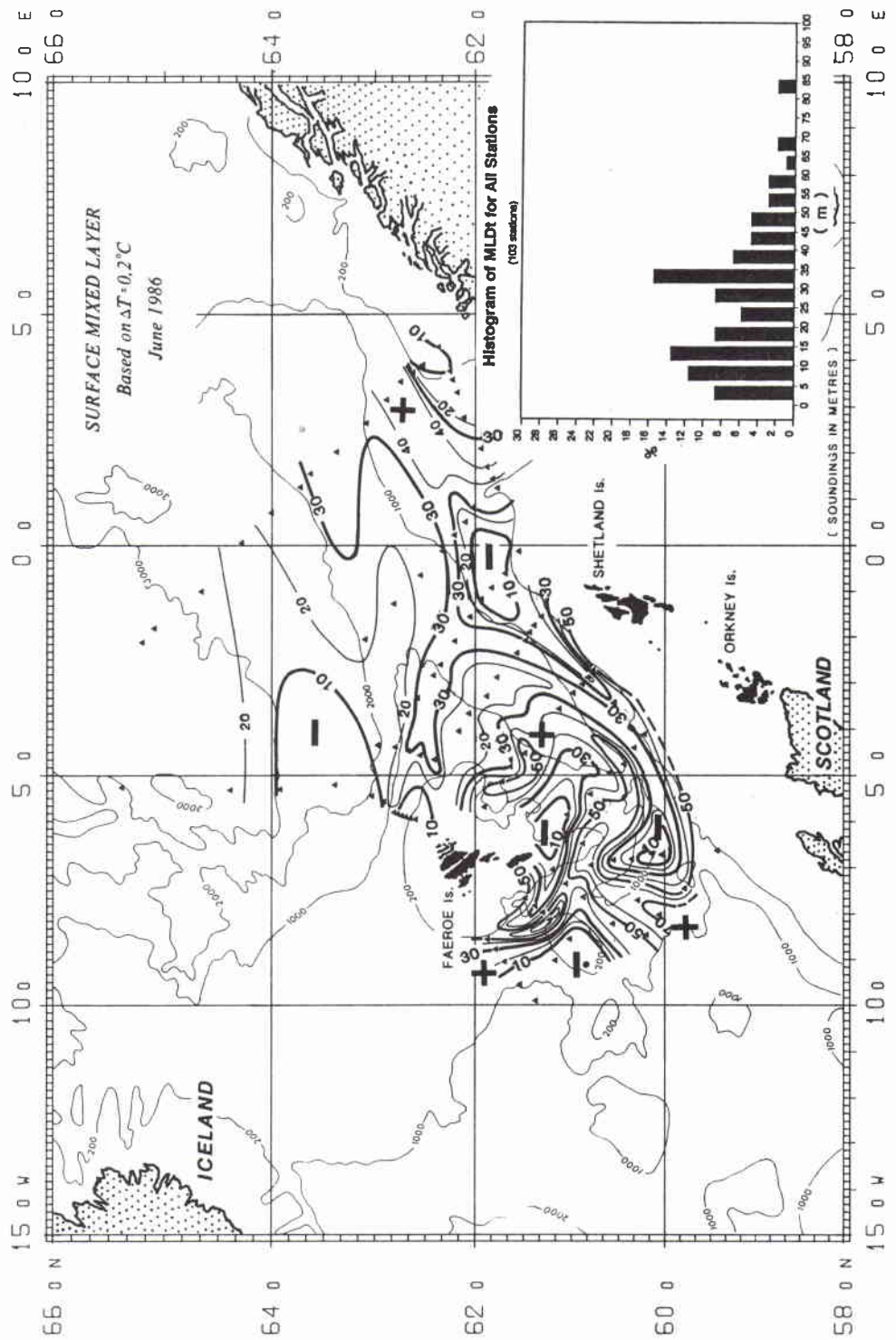


**Figure 7** *The distribution of the* MLD *as determined by the temperature, with the insert displaying the percentage distribution.*

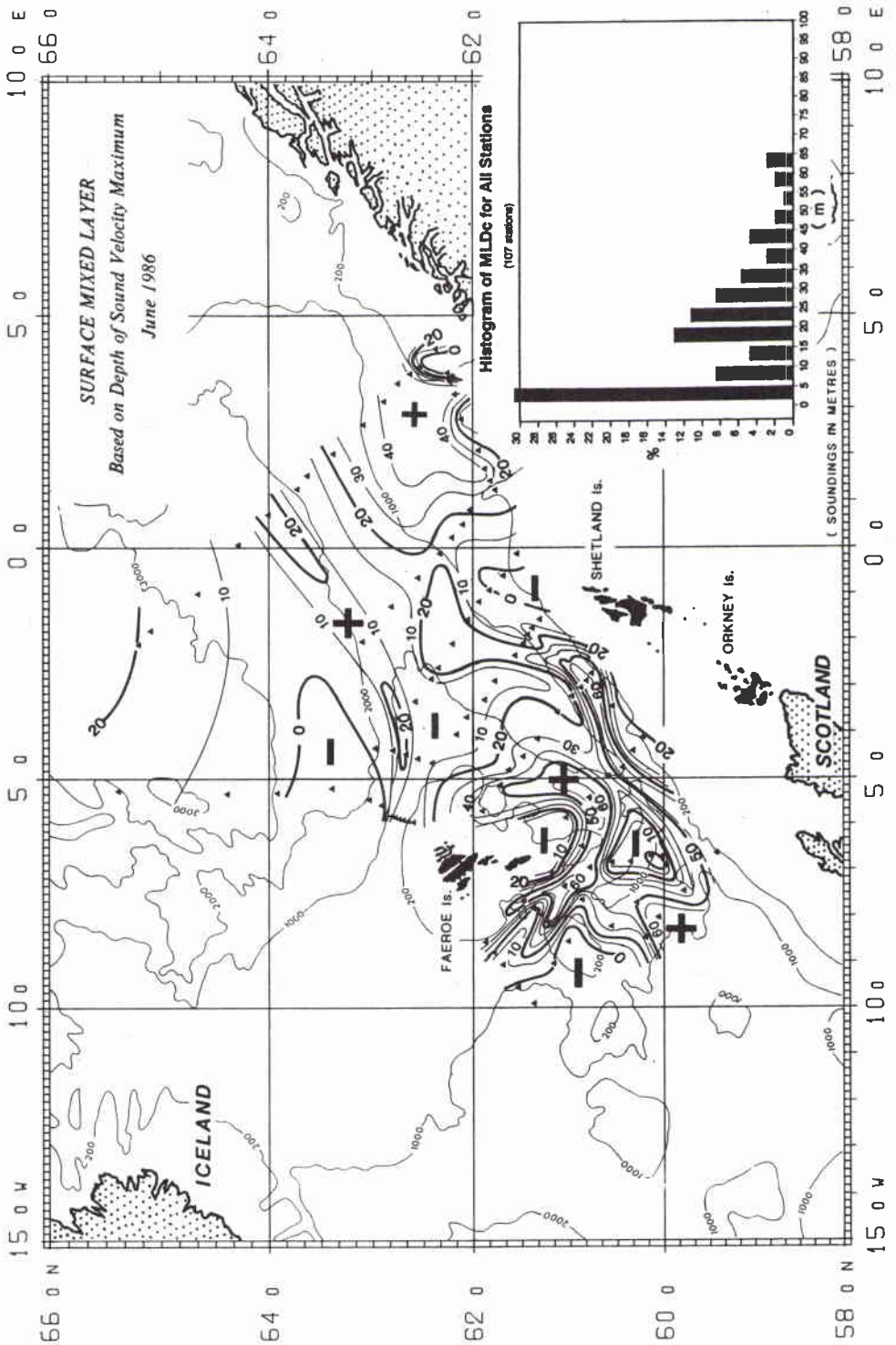


**Figure 8** *The distribution of the* MLD *as determined by the sound-velocity maximum, with the insert displaying the percentage distribution.*

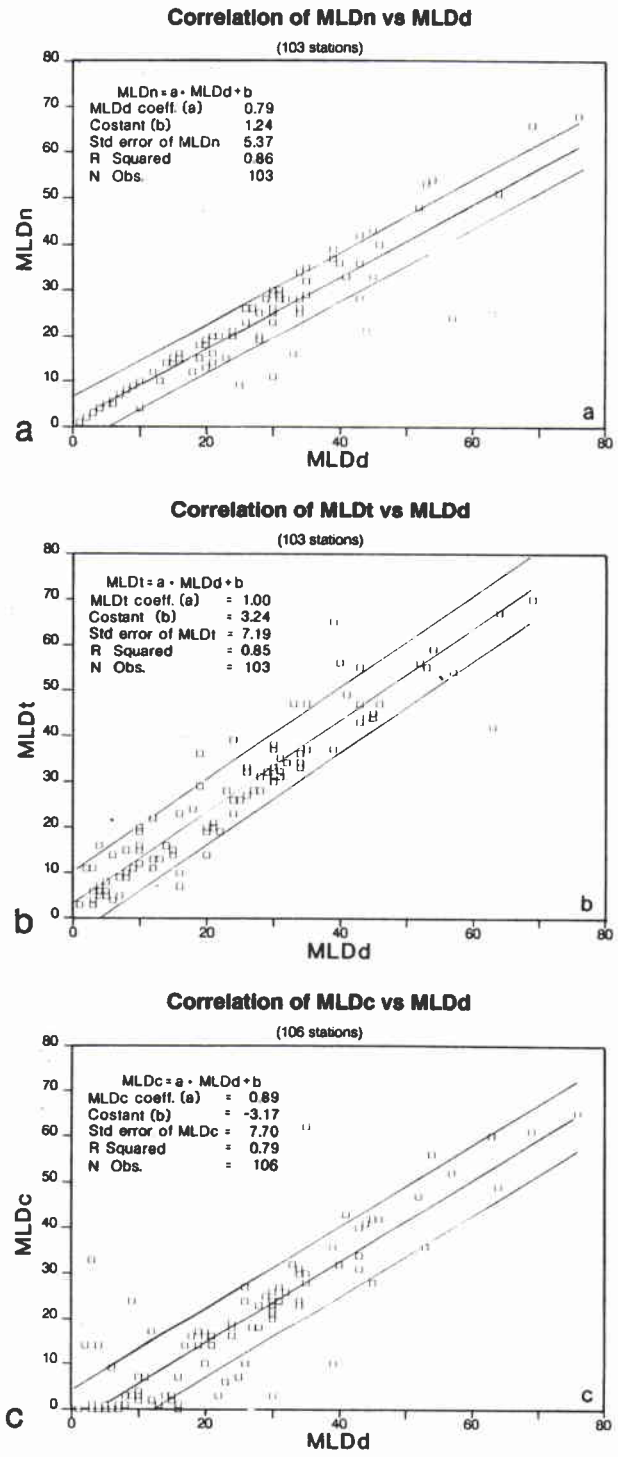


**Figure 9** *The correlation between* $MLD_d$ *and (a)* $MLD_N$, *(b)* $MLD_t$, *(c)* $MLD_c$.

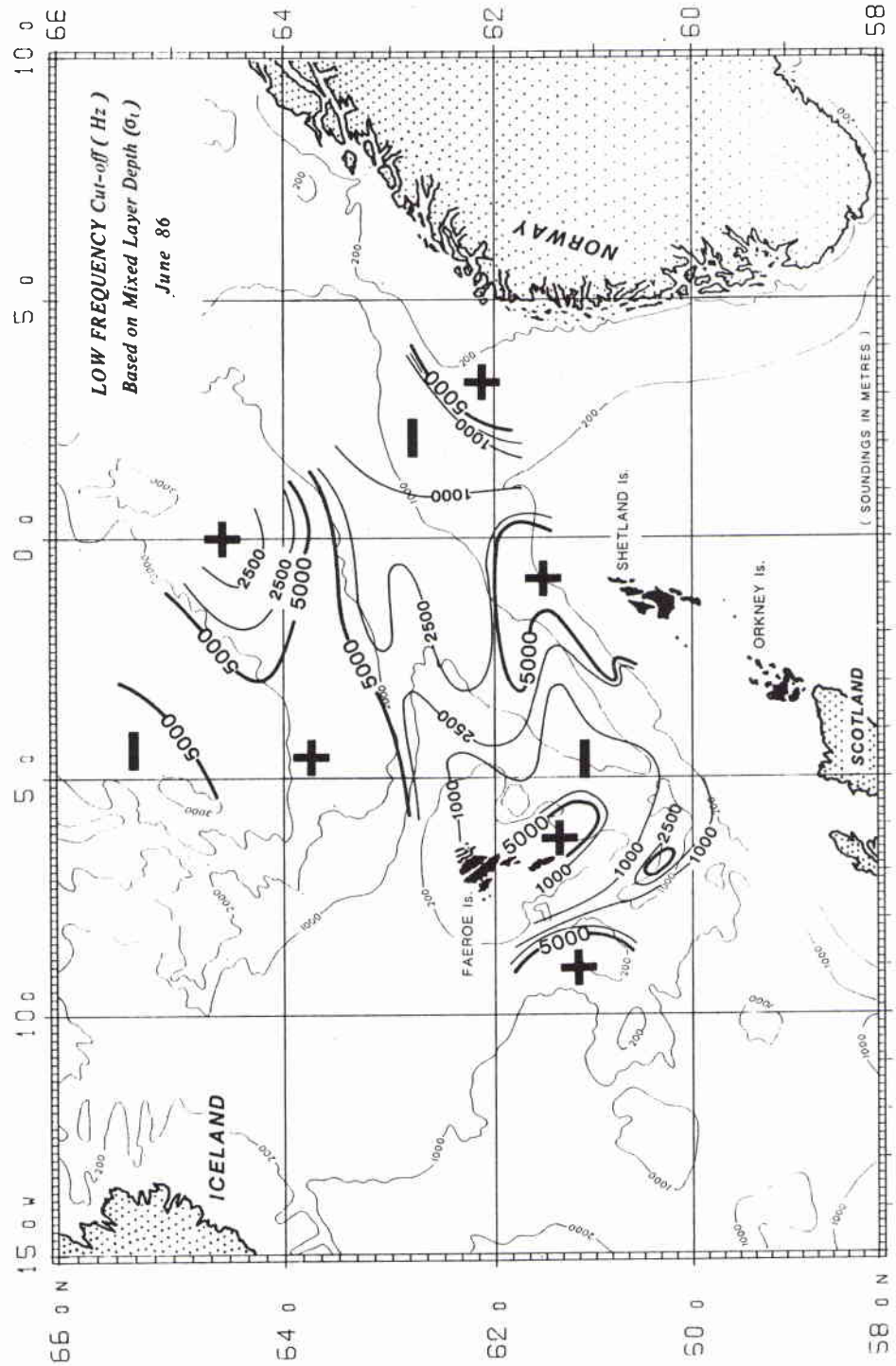


**Figure 10** *The distribution of the low-frequency cut-off for the trapping of sound in the surface layer, based on* $MLD_d$.

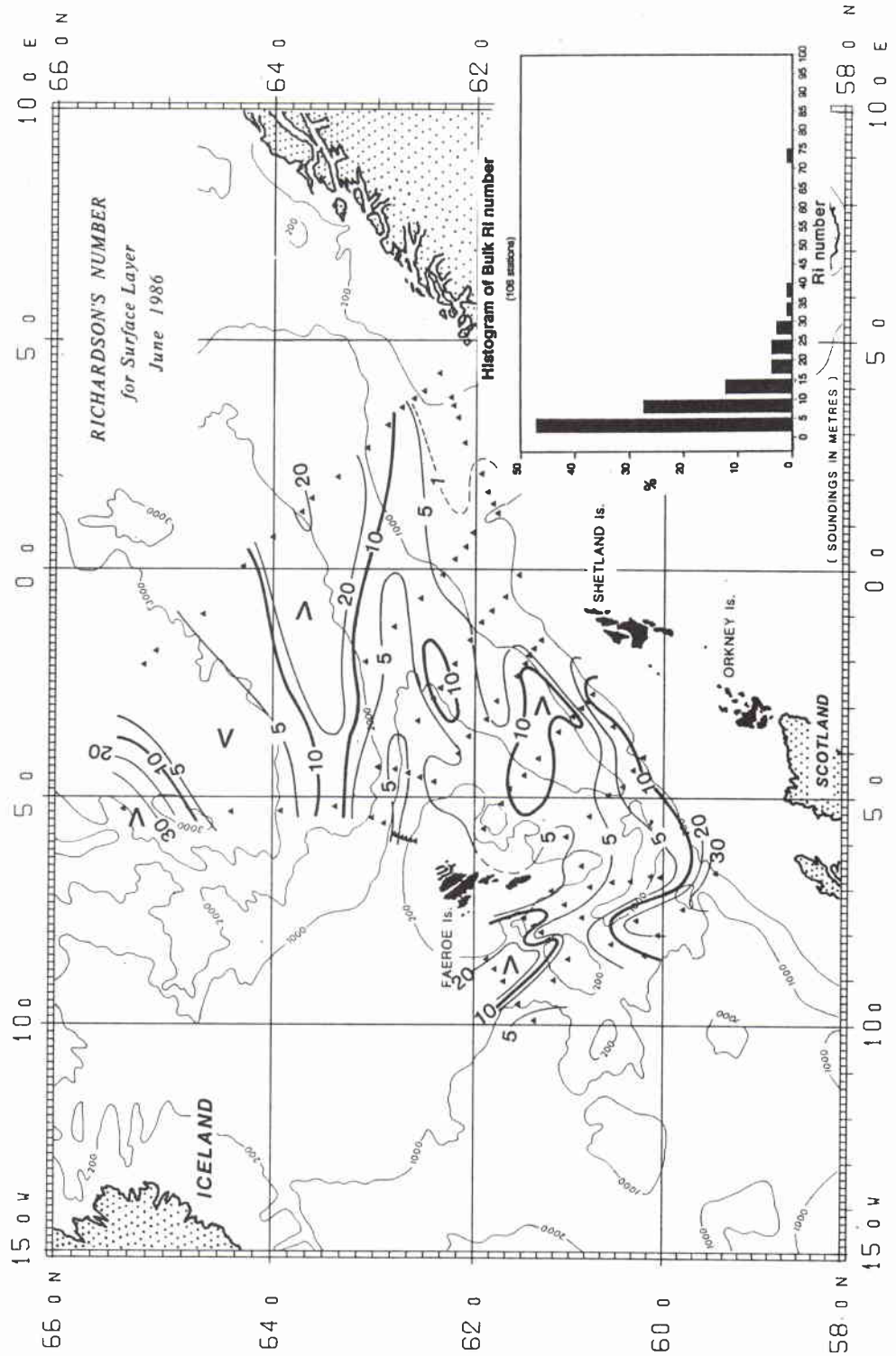


**Figure 11** *The distribution of the bulk Richardson number.*

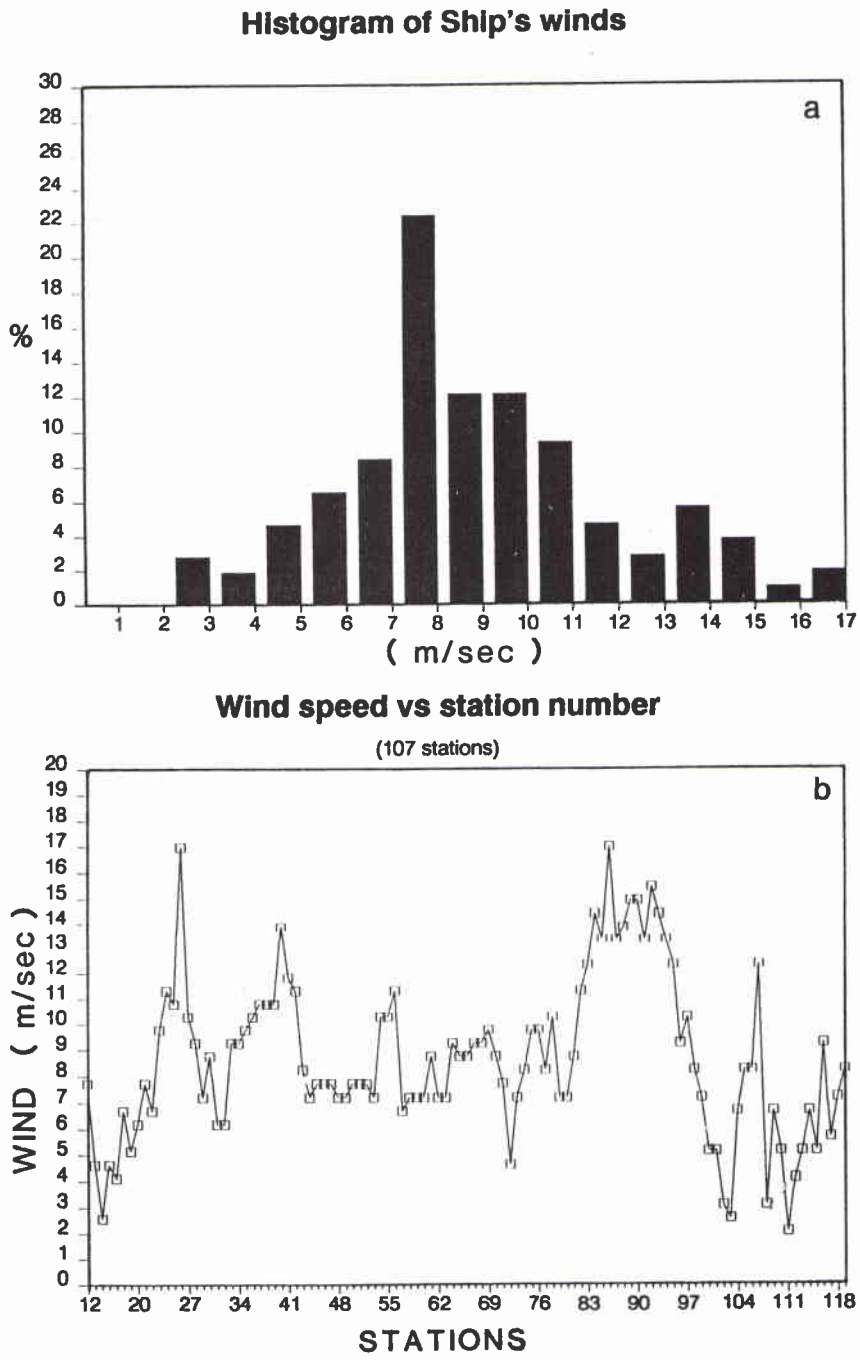


**Figure 12** *The frequency distribution of the ship's observed winds.*

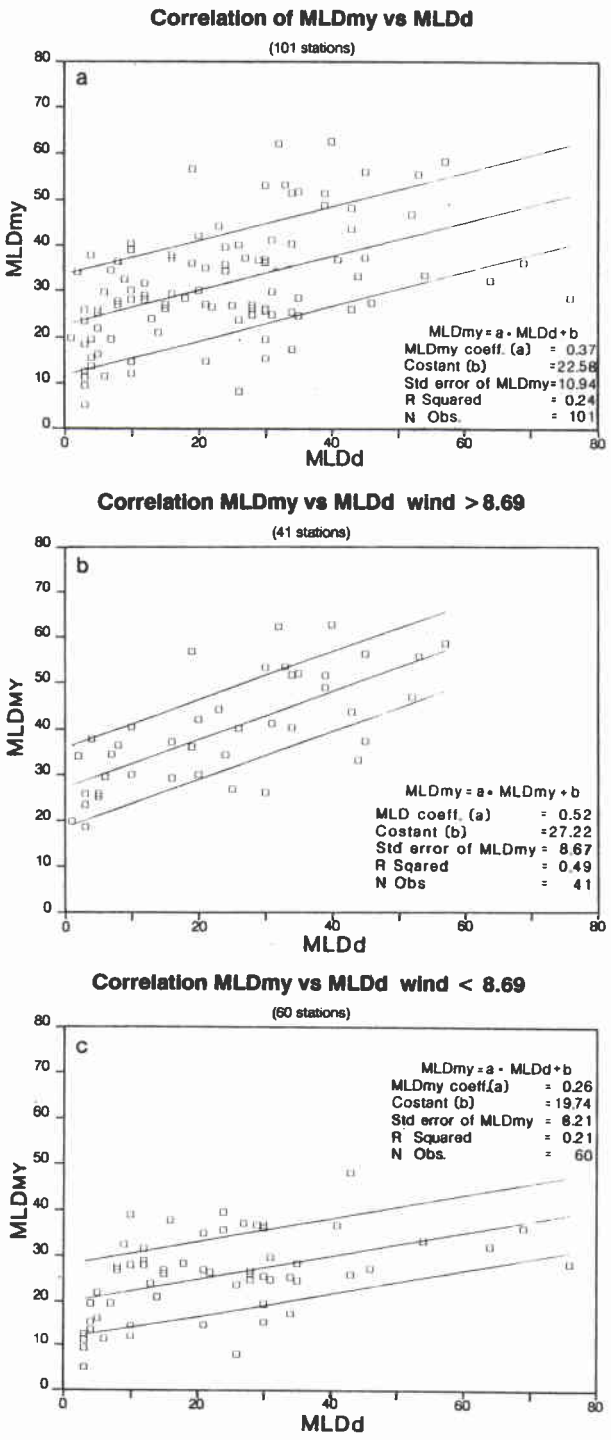


**Figure 13** *(a) A scatter plot showing the correlation between the calculated* $MLD_{MY}$ *values and the observed values of* $MLD_d$*. (b) The same for the stations having winds greater than 8.7 m/s. (c) The same for winds less than 8.7 m/s.*

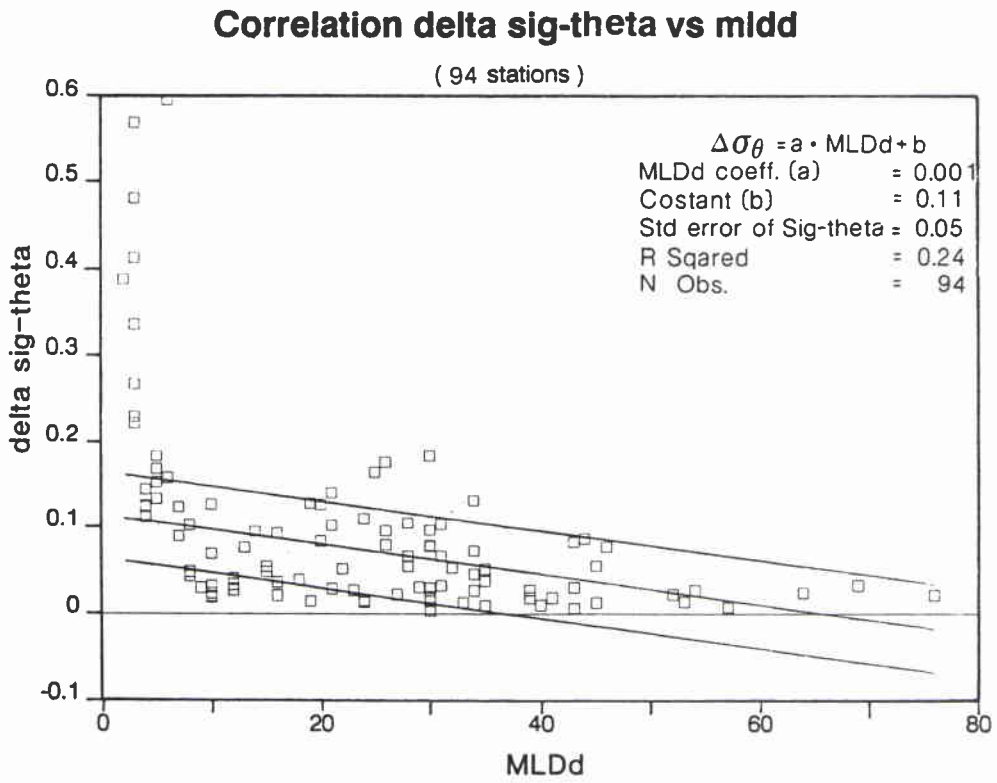


**Figure 14** *A scatter plot of the values of the 10-m density gradient just below* MLD *and* $MLD_d$.

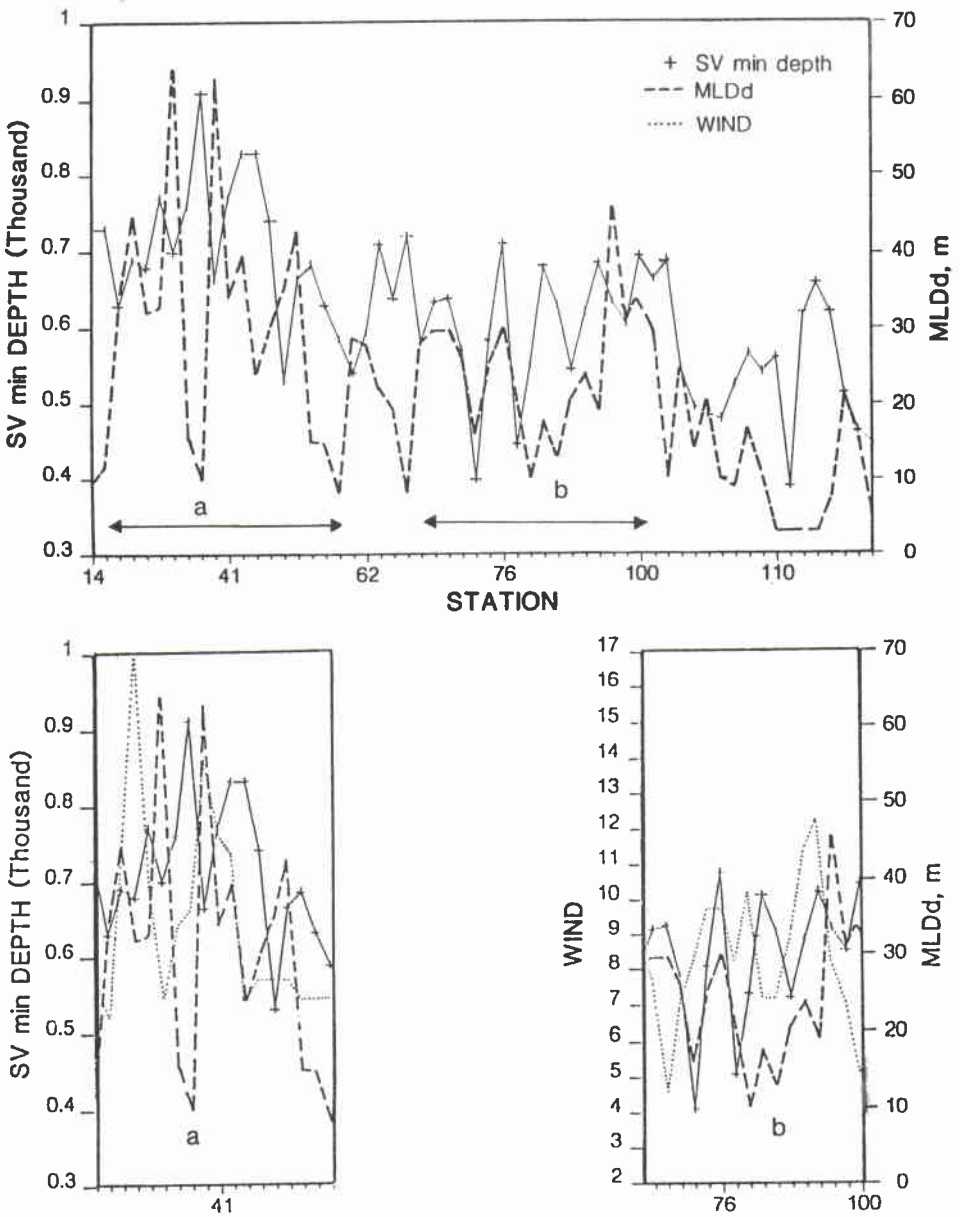


**Figure 15** *A comparison of the depths of the* $SV_{min}$ *and* $MLD_d$ *for Region 1. Panels (a) and (b) present expanded sections of the same plot along with the observed wind.*

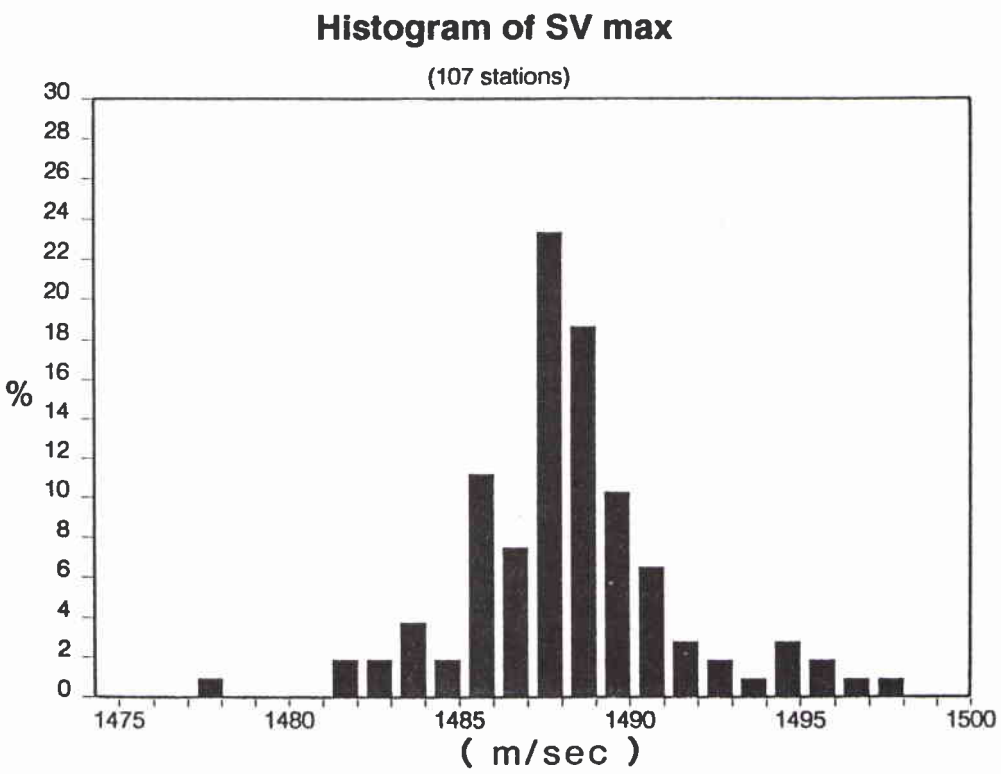


**Figure 16** *A historgam of the* $SV_{max}$.

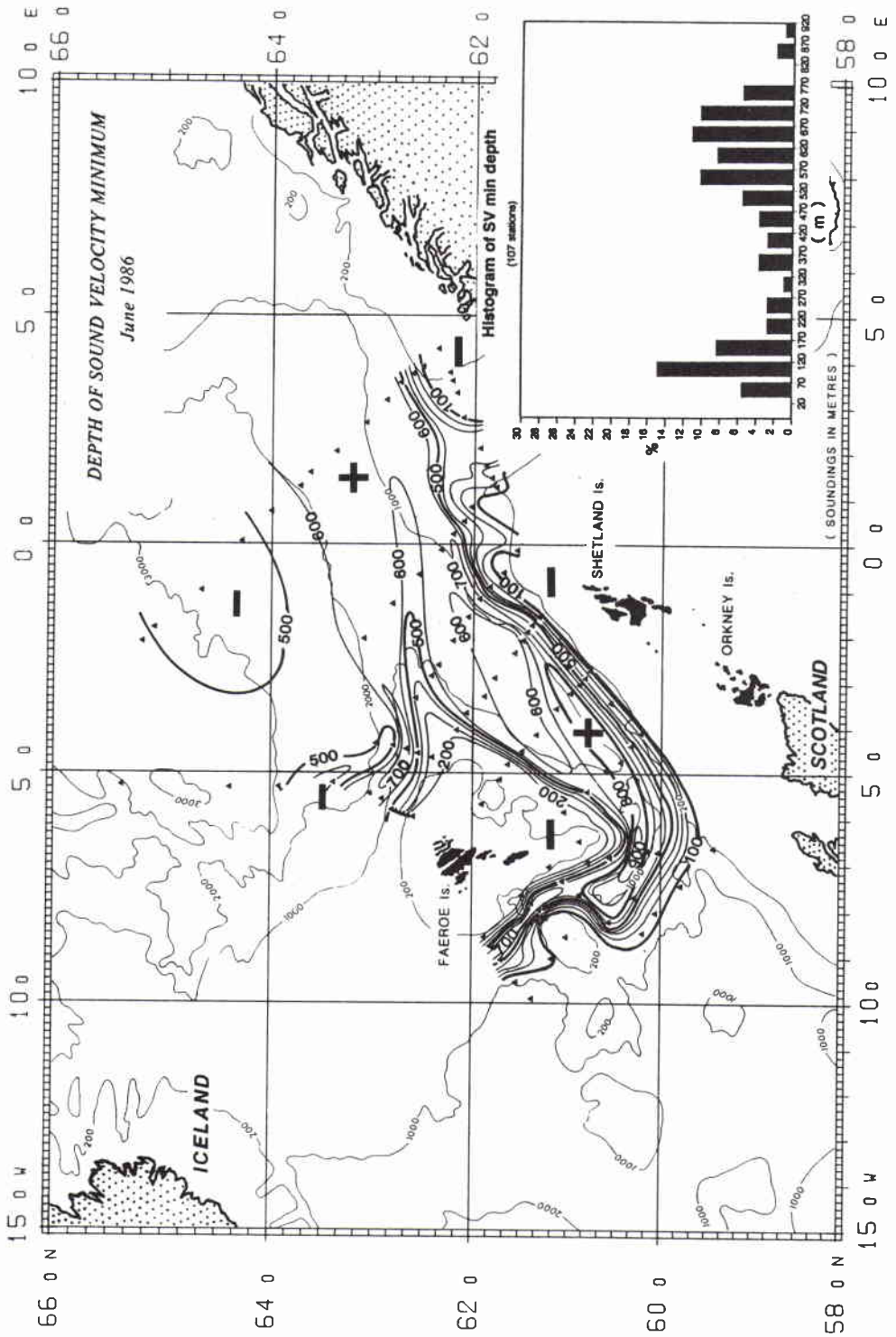


**Figure 17** *The distribution of the depth of the sound-velocity minimum with a histogram shown in the insert.*

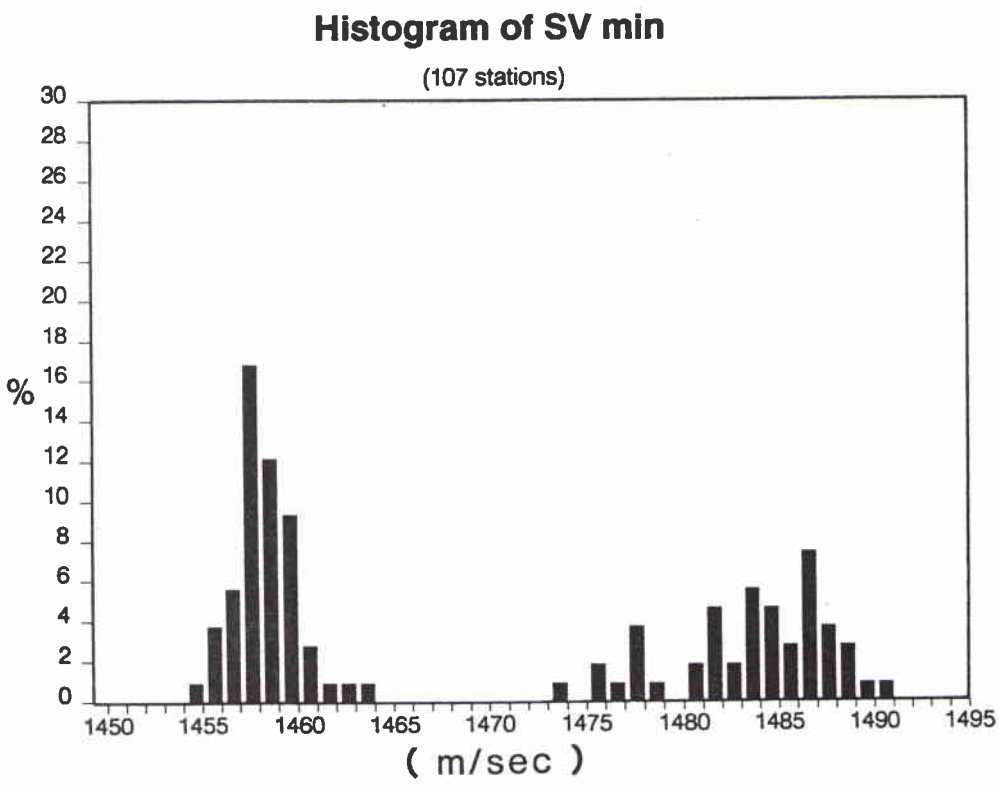


**Figure 18** *A histogram of the* $SV_{min}$.

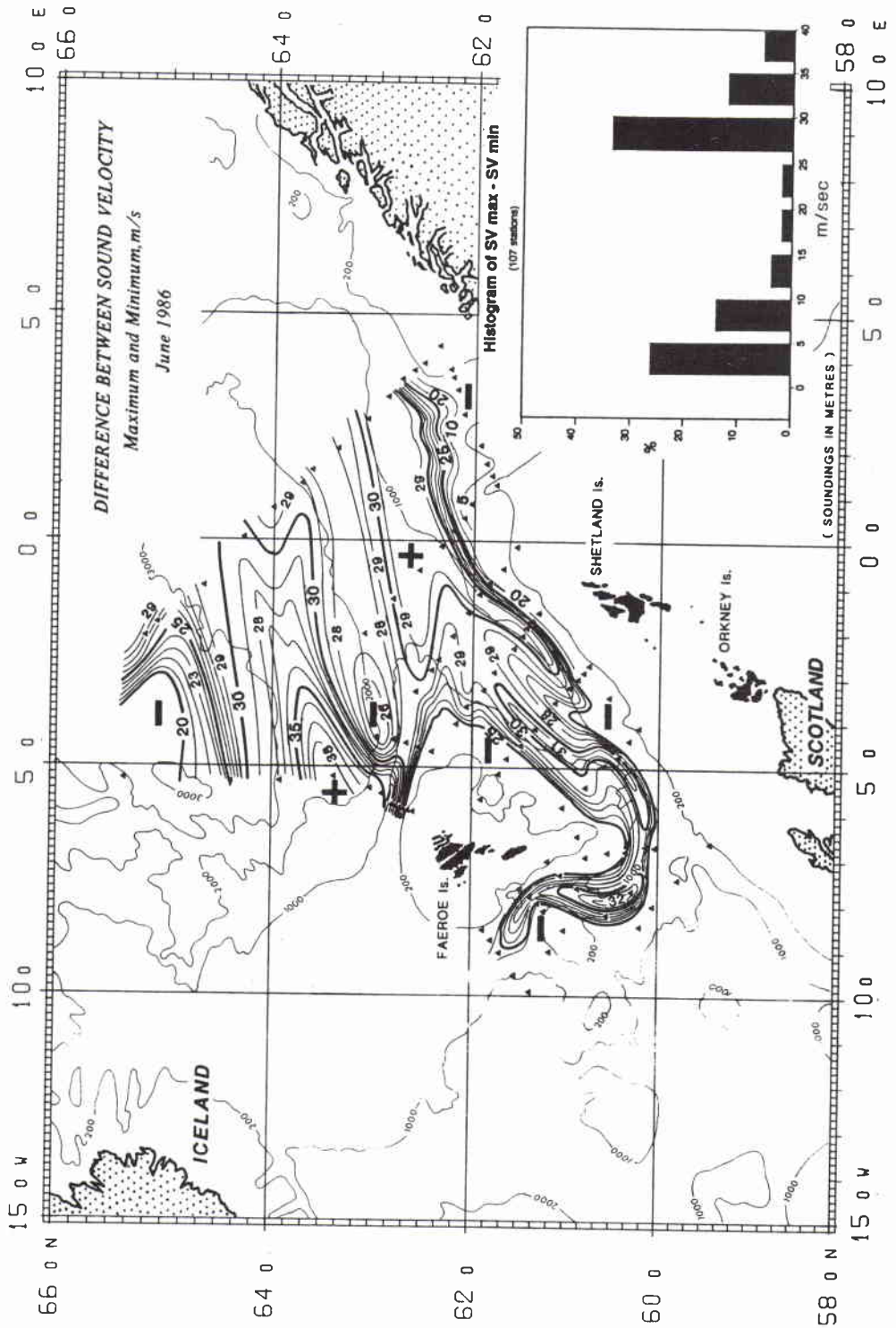


**Figure 19** *The distribution of the difference between the* $SV_{max}$ *and the* $SV_{min}$ *(in m/s) with a histogram shown in the insert.*

## Initial Distribution for SM-225

| | |
|---|---|
| *Ministries of Defence* | |
| JSPHQ Belgium | 2 |
| DND Canada | 10 |
| CHOD Denmark | 8 |
| MOD France | 8 |
| MOD Germany | 15 |
| MOD Greece | 11 |
| MOD Italy | 10 |
| MOD Netherlands | 12 |
| CHOD Norway | 10 |
| MOD Portugal | 5 |
| MOD Spain | 2 |
| MOD Turkey | 5 |
| MOD UK | 20 |
| SECDEF US | 60 |
| *NATO Authorities* | |
| Defence Planning Committee | 3 |
| NAMILCOM | 2 |
| SACLANT | 3 |
| SACLANTREPEUR | 1 |
| CINCWESTLANT/ COMOCEANLANT | 1 |
| COMSTRIKFLTANT | 1 |
| CINCIBERLANT | 1 |
| CINCEASTLANT | 1 |
| COMSUBACLANT | 1 |
| COMMAIREASTLANT | 1 |
| SACEUR | 2 |
| CINCNORTH | 1 |
| CINCSOUTH | 1 |
| COMNAVSOUTH | 1 |
| COMSTRIKFORSOUTH | 1 |
| COMEDCENT | 1 |
| COMMARAIRMED | 1 |
| CINCHAN | 3 |
| *SCNR for SACLANTCEN* | |
| SCNR Belgium | 1 |
| SCNR Canada | 1 |
| SCNR Denmark | 1 |
| SCNR Germany | 1 |
| SCNR Greece | 1 |
| SCNR Italy | 1 |
| SCNR Netherlands | 1 |
| SCNR Norway | 1 |
| SCNR Portugal | 1 |
| SCNR Turkey | 1 |
| SCNR UK | 1 |
| SCNR US | 2 |
| SECGEN Rep. SCNR | 1 |
| NAMILCOM Rep. SCNR | 1 |
| *National Liaison Officers* | |
| NLO Canada | 1 |
| NLO Denmark | 1 |
| NLO Germany | 1 |
| NLO Italy | 1 |
| NLO UK | 1 |
| NLO US | 1 |
| *NLR to SACLANT* | |
| NLR Belgium | 1 |
| NLR Canada | 1 |
| NLR Denmark | 1 |
| NLR Germany | 1 |
| NLR Greece | 1 |
| NLR Italy | 1 |
| NLR Netherlands | 1 |
| NLR Norway | 1 |
| NLR Portugal | 1 |
| NLR Turkey | 1 |
| NLR UK | 1 |
| Total external distribution | 236 |
| SACLANTCEN Library | 10 |
| Stock | 34 |
| Total number of copies | 280 |